Enhanced Output from Biohybrid Photoelectrochemical Transparent Tandem Cells Integrating Photosynthetic Proteins Genetically Modified for Expanded Solar Energy Harvesting

*Sai Kishore Ravi, Zhimeng Yu, David J. K. Swainsbury, Jianyong Ouyang, Michael R. Jones, and Swee Ching Tan**

Increased solar energy utilization has been forecast as the principal way to meet the growing energy demands of the 21st century in an environmentally benign way. In response, significant efforts are being made to develop novel and cost-effective approaches to solar energy conversion that do not compromise environmental security.[1] Given that photosynthesis is the prime process that powers the biosphere,[2,3] the strategies of emulating and directly exploiting natural photosynthetic machineries for solar energy harvesting have attracted substantial interest in recent years.[4,5] At the heart of the photosynthetic process, reaction center (RC) and light harvesting (LH) pigment–protein complexes accomplish the transduction of absorbed light energy through a photochemical charge separation in which an electron is generated for almost every photon absorbed.[5,6] The photosynthetic pigment–proteins of plants, algae, and bacteria have therefore been evaluated for a range of potential optoelectronic, bioelectronic, and photo-bioelectrochemical devices and applications.[7,8]

RCs from purple photosynthetic bacteria such as *Rhodobacter* (*Rba.*) *sphaeroides*,[9] and the larger RC–LH1 complexes they form with the LH1 light harvesting protein,[10] are a popular choice for the construction of photo-bioelectrochemical cells.[7,11,12] Previous studies utilizing these proteins have been aimed at enhancing photocurrent generation by improving the effectiveness of protein–electrode electron transfer processes in three-electrode cells[13] or, to a lesser extent, in two-electrode cells.[14,15] Manipulating protein orientation and the nature of chemical or biochemical linkers for immobilizing proteins on electrodes has been the primary approach to improving electron-transfer, along with the use of alternative electrode/electrolyte combinations based on energy-level considerations to achieve current enhancement (see refs. [7,11] for reviews). In contrast, there have been almost no attempts to enhance photocurrents by augmenting the natural light-harvesting abilities of photosynthetic bacteria and therefore the spectral range covered in biohybrid devices. A characteristic of natural photosynthetic pigments is that they have strong absorbance bands in some regions of the UV–visible–near-IR spectrum but little or no absorbance in other regions. Plasmonic enhancement of photocurrent generation by purple bacterial RC–LH1 complexes on nanostructured metal electrodes has been achieved,[16] but this does not change the wavelengths of light absorbed. A few attempts have been made to increase the optical absorption cross-section of photosynthetic RCs or LH complexes by attaching tailored molecular fluorophores and photoluminescent quantum dots, but these have not been scaled up for photocurrent generation at a device-level.[17] Fabrication of such partially-synthetic photovoltaic proteins complicates device construction, adds to cost, and can involve the use of materials that are not environmentally friendly or constitute a limited resource.

An alternative approach to enhancing spectral coverage is to employ a stacked tandem device architecture in which photovoltaic proteins with natural pigments that have complementary absorption characteristics incorporated into different layers of the device. Here we employ two variants of RC–LH1 complexes which incorporate either the native red carotenoid spheroidenone (RC–LH1$_{red}$) or the green carotenoids neurosporene, hydroxyneurosporene, and methoxyneurosporene (RC–LH1$_{green}$) (**Figure 1**a–c). This is achieved using a "green strain" of *Rba. sphaeroides* containing a spontaneous mutation in the *crtD* gene encoding methoxyneurosporene dehydrogenase, which halts carotenoid synthesis prematurely.[18] The two, otherwise identical, pigment–proteins have different absorption characteristics in the blue to yellow region of the visible spectrum (Figure 1d,e and Figure S1 in the Supporting Information), 17 molecules of spheroidenone per complex giving rise to a single broad band between 400 and 600 nm, and 17 molecules of neurosporene and its derivatives to narrower, more intense absorbance between 400 and 500 nm with distinctive maxima at 429, 454, and 485 nm.[19] As the tandem cell architecture requires a transparent rear electrode for the front cell, we have explored the option of using poly(3,4-ethylenedioxythiophene): polystyrene sulfonate (PEDOT:PSS). This transparent polymer

S. K. Ravi, Z. Yu, Prof. J. Ouyang, Prof. S. C. Tan
Department of Materials Science and Engineering
National University of Singapore
9 Engineering Drive 1, Singapore 117575, Singapore
E-mail: msetansc@nus.edu.sg
Dr. D. J. K. Swainsbury, Dr. M. R. Jones
School of Biochemistry
Biomedical Sciences Building
University of Bristol
University Walk
Bristol BS8 1TD, UK

DOI: 10.1002/aenm.201601821

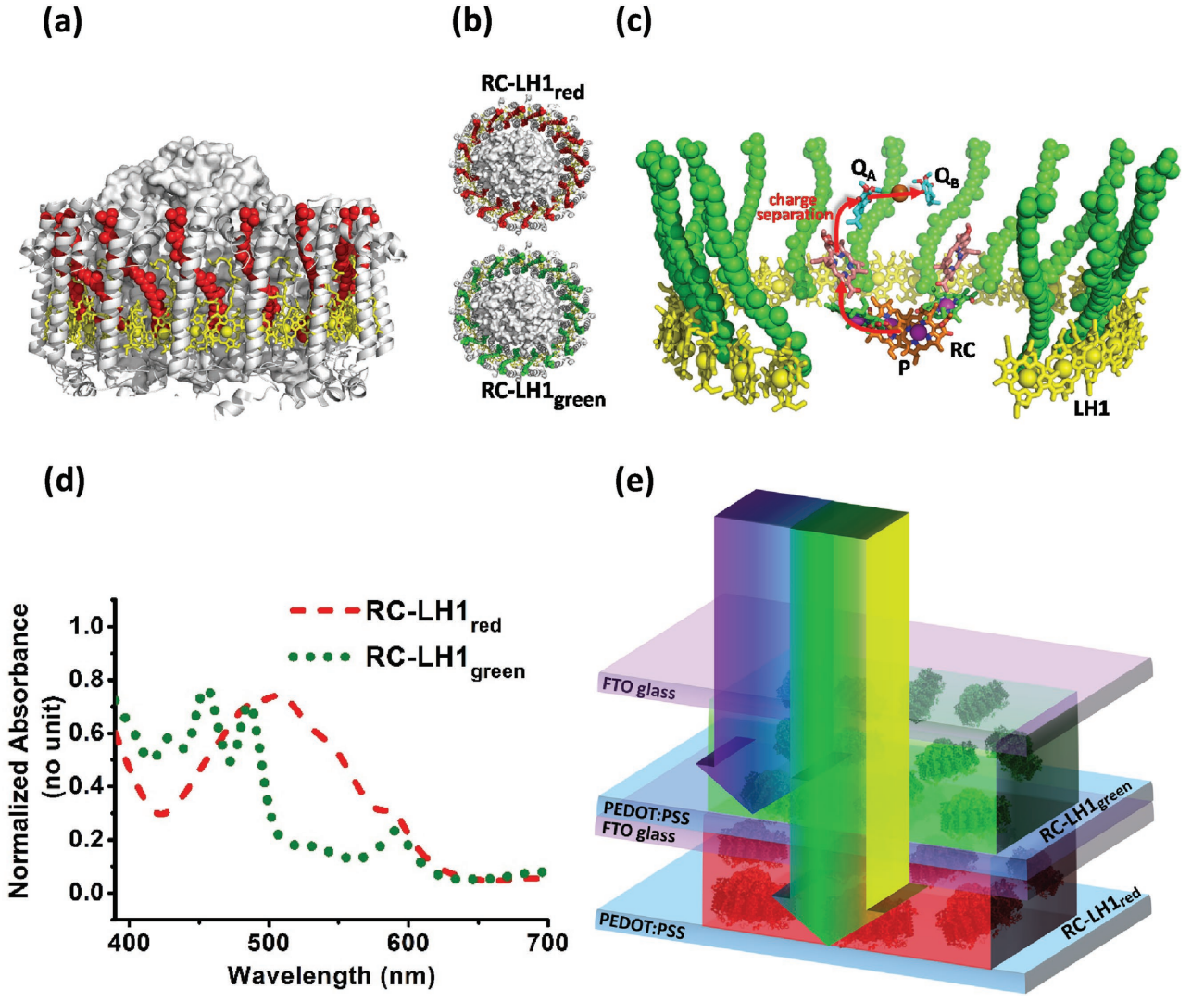

Figure 1. Molecular models and absorbance properties of RC-LH1$_{red}$ and RC-LH1$_{green}$ complexes. a) RC-LH1$_{red}$ complex viewed parallel to the photosynthetic membrane, with the 16 LH1 carotenoids carotenoid shown as red spheres, LH1 BChls in yellow and all other components in white. The RC is shown as a solid object and LH1 proteins as ribbons. Other details of the models are described in the Experimental Section. b) Views of RC-LH1$_{red}$ and RC-LH1$_{green}$ complexes perpendicular to the photosynthetic membrane; only the carotenoid pigments differ between complexes. c) The LH1 carotenoids (green) and BChls (yellow) power charge separation in the central RC by passing excited state energy to the P BChls (orange carbons). The nearest four BChls and two carotenoids have been removed (For clearer structural details and color codes of the proteins, refer S1 a-d, Supporting Information). d) Visible region absorbance spectra of RC-LH1$_{red}$ and RC-LH1$_{green}$ complexes in solution, normalised to BChl absorbance at 875 nm (Figure S1 in Supporting Information). e) Schematic of a tandem device architecture for enhanced light-harvesting with the complementary absorption in blue to yellow region. Illumination was from the top and sub-cells were connected in parallel (Figure S4).

has attracted considerable interest in photovoltaics owing to its good electronic conductivity achievable on chemical treatment and also due to its low cost.[20] To our knowledge, PEDOT:PSS has not so far been evaluated as an electrode material in a protein based photo-bioelectrochemical cell.

In this work, optically-complementary RC–LH1$_{red}$ and RC–LH1$_{green}$ proteins were encapsulated in subcells formed from a sandwich of fluorine-doped tin oxide (FTO) glass and PEDOT:PSS electrodes, and assembled either individually or in a tandem architecture. By measuring photocurrents from a variety of cell configurations, we demonstrate current enhancements brought about by the tandem architecture and the advantages of using transparent polymeric electrode materials.

Subcells were constructed by connecting front FTO glass and rear PEDOT:PSS electrodes with a 50 µm thick U-shaped thermoplastic spacer. Tandem cells were constructed with a middle electrode comprising an FTO glass substrate with PEDOT:PSS coated on the non-conductive side (Figure 1e). The conductive PEDOT:PSS films prepared by two rounds of spin coating had a smooth and homogeneous topography (**Figure 2**) with a root-mean-square roughness of ≈1 nm, a mean thickness of 34 ± 4 nm and a transmittance of 93% at 550 nm. Consistent smoothness of these surfaces is known to be favorable for application as electrode materials in several electronic devices.[21] Further thickening the PEDOT:PSS layer negatively impacted on transparency which is unfavorable for a tandem architecture

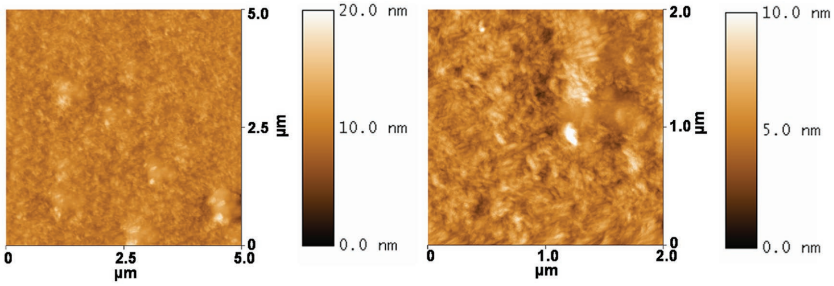

Figure 2. AFM topograms of the PEDOT:PSS film over 25 µm^2 (left) and 4 µm^2 (right) areas.

(Figure S2 in the Supporting Information). Given the purpose of the present study of testing a transparent tandem architecture, cells with a thin PEDOT:PSS layer were used to achieve optimal transparency. Solutions of 50×10^{-6} M protein injected into the cavity of each subcell included 10×10^{-3} M ubiquinone-0 (Q_0) and 1×10^{-3} M N,N,N′,N′-tetramethyl-p-phenylenediamine (TMPD) as electrolytes.[14] Assembled subcells and tandem cells were visibly transparent (**Figure 3**), with transmittances at 550 nm of 82% for the RC–LH1$_{red}$ subcell (Figure 3b) and 87% for the RC–LH1$_{green}$ subcell (Figure 3a). The lower transmittance of the former was consistent with the higher absorbance of spheroidene at this wavelength compared to neurosporene (Figure 1d). A green/red (top/bottom) tandem cell (Figure 3c) had a transmittance at 550 nm of 59%, intermediate between that of a green/green tandem cell (61%) and a red/red tandem cell (56%), and again consistent with the higher absorbance of spheroidenone at 550 nm. Both the electrode materials (FTO and PEDOT:PSS) had a very minimal absorbance in the range of 400–600 nm where the two proteins exhibit complementary absorption characteristics (Figure S3, Supporting Information). All cells were two terminal devices (Figure 1e and Figure S4, Supporting Information). In the case of the tandem cell both front electrodes were connected together as were both back electrodes (Figure S4c, Supporting Information), producing a parallel architecture.

Our previous work on photocurrent generation by RC–LH1$_{red}$ complexes employed Platinum (Pt) as the rear electrode material.[14] In the present work, both red and green subcells with PEDOT:PSS as the rear electrode showed significantly higher average steady-state photocurrents (≈5 µA cm^{-2}—**Figure 4**a) compared with identical cells made with a 25 nm thick Pt rear electrode (0.3–0.4 µA cm^{-2}—Figure 4a). In addition to being more cost-effective therefore, PEDOT:PSS was also a more functionally effective alternative to Pt for collection of electrons following charge separation in the photoactive proteins.

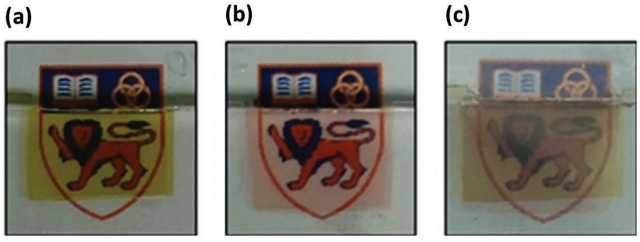

Figure 3. Active areas of sub-cells and a tandem cell on a coloured background. a) Sub-cell with RC-LH1$_{green}$, b) sub-cell with RC-LH1$_{red}$, c) green/red tandem cell.

Measurements of red/red and green/green tandem cells fabricated with PEDOT:PSS demonstrated the drawbacks of adding more layers of an optically-identical material in an attempt to obtain larger photocurrents from a given footprint. Over multiple measurements (Figure 4d) the photocurrents obtained from these tandem cells were only 44% (red/red) and 59% (green/green) larger than currents obtained from the equivalent single subcells. This demonstration of the law of diminishing returns caused us to explore a tandem architecture in which higher-energy absorbing RC–LH1$_{green}$ complexes were stacked on top of lower-energy absorbing RC–LH1$_{red}$ complexes. One such green/red tandem cell exhibited a maximum peak current density of ≈58 µA cm^{-2} and a steady-state photocurrent density of ≈8.6 µA cm^{-2} (Figure 4a inset). Over multiple measurements this steady state output was ≈74% greater than the steady-state photocurrent density produced by either the red and green subcells (see Figure 4a, inset), and this current increase was significantly higher than could be achieved from green/green or red/red tandem cells (Figure, 4c, inset).

To further examine possible benefits of the controlled heterogeneity offered by the tandem structure, a cell was prepared with an equimolar mixture of red and green RC–LH1 proteins, the individual concentrations being the same as used for the component proteins in the green/red tandem cell. This "mixed cell" yielded a ≈41% lower photocurrent compared to the green/red tandem cell (Figure 4a, inset). This lower photocurrent is attributed to shading of green complexes by red complexes in the mixed cell configuration. The green/red tandem cell and the two corresponding subcells produced average steady-state open-circuit photovoltages of ≈3 mV, with only a negligible difference of 0.1 mV between the two subcells (Figure 4b). The factors that give rise to this voltage, including the potentials of the electron transfer components with the RC–LH1 complex, are not expected to be affected by the type of carotenoid present.

In exploring ways to supplement the tandem effect, a tandem cell with a higher protein loading was tested. To avoid any absorption losses caused by shading by the top cell the protein loading was doubled only in the bottom RC–LH1$_{red}$ cell. Experiments with subcells containing RC–LH1$_{green}$ complexes at 50×10^{-6} M and RC–LH1$_{red}$ complexes at 100×10^{-6} M showed that doubling the RC–LH1$_{red}$ concentration boosted the current output by ≈50% (Figure S5, Supporting Information). However in the tandem architecture, doubling the RC–LH1$_{red}$ concentration in the lower cell to 100×10^{-6} M produced a photocurrent that was increased by only ≈20% compared to previous green/red tandem cells with a 50×10^{-6} M concentration for both proteins (Figure S5, Supporting Information & Figure 4a). Doubling the RC–LH$_{red}$ concentration in the lower cell resulted in a lower overall transmittance of 38% (Figure S6, Supporting Information), indicating the constraint of maintaining the transparency of the cells for practical applications and the need for a trade-off between the transmittance and photocurrent in such devices.

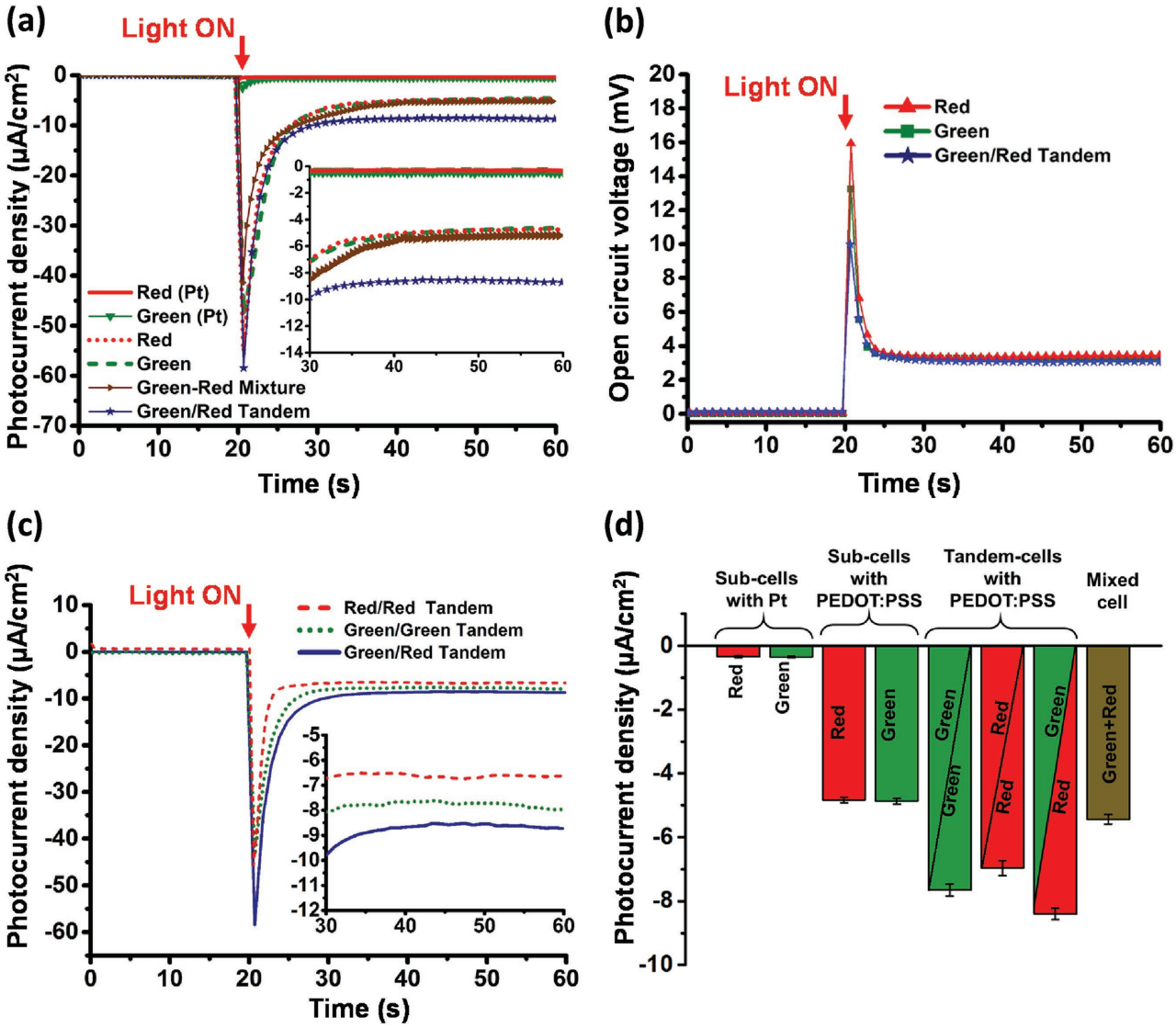

Figure 4. Output of sub-cells and tandem cells. a) Photocurrent density from green and red sub cells with either PEDOT:PSS or Pt back electrodes, a green/red mixture cell and a green/red tandem cell. b) Open circuit voltage from green and red sub-cells and a green/red tandem cell. c) Comparison of photocurrent density from tandem cells with green/green, red/red and green/red configurations. d) Comparison of steady-state photocurrent densities produced by the sub-cells, tandem cells and the mixed cell with mean photocurrents (average ± standard error; $n = 3$ cells; All the measurements were performed using a solar simulator with a standard light intensity of 100 mW cm^{-2} under AM 1.5 conditions).

External quantum efficiency (EQE) action spectra were measured to confirm the source of photocurrent and to further demonstrate the photocurrent enhancement resulting from the improved light absorption cross-section in the tandem cell (**Figure 5**a). These showed bands at 375, 600, and above 700 nm attributable to the RC–LH1 bacteriochlorophyll (BChl) pigments. Bands at 805 and 875 nm are attributable to the BChls of the RC and the surrounding LH1 ring, respectively. In the 430–580 nm region the EQE spectrum of the green/red tandem cell showed spectral features attributable to the carotenoids in the green, upper cell between 430 and 510 nm and the red, lower cell in the region around 560 nm. A maximum EQE at 870 nm of 1.3% was obtained for the green/red tandem cell, while the individual green and red subcell had an EQE of 1.1% and 0.85%, respectively, at this wavelength (Figure 5a).

The tandem cells showed reasonable stability under continuous illumination for a protein-based photoelectrochemical cell, exhibiting ≈40% of the original current density after 4 h of continuous illumination (Figure S7, Supporting Information).

The suggested mechanism for photocurrent generation is shown in Figure 5b. Photo-oxidation of the primary electron donor BChls in the RC (P→P*), principally following excitation transfer from the BChls and carotenoids of the LH1 antenna, results in charge separation to reduce the Q_B ubiquinone. In line with previous studies,[14] maximal photocurrents were obtained using a mixture of Q_0 and TMPD. It is likely that Q_0 enhanced electron transfer from the Q_B quinone binding site to the rear electrode whilst TMPD mediated between the front electrode and the photo-oxidized RC. Another salient point is that PEDOT:PSS presents less of a potential drop for

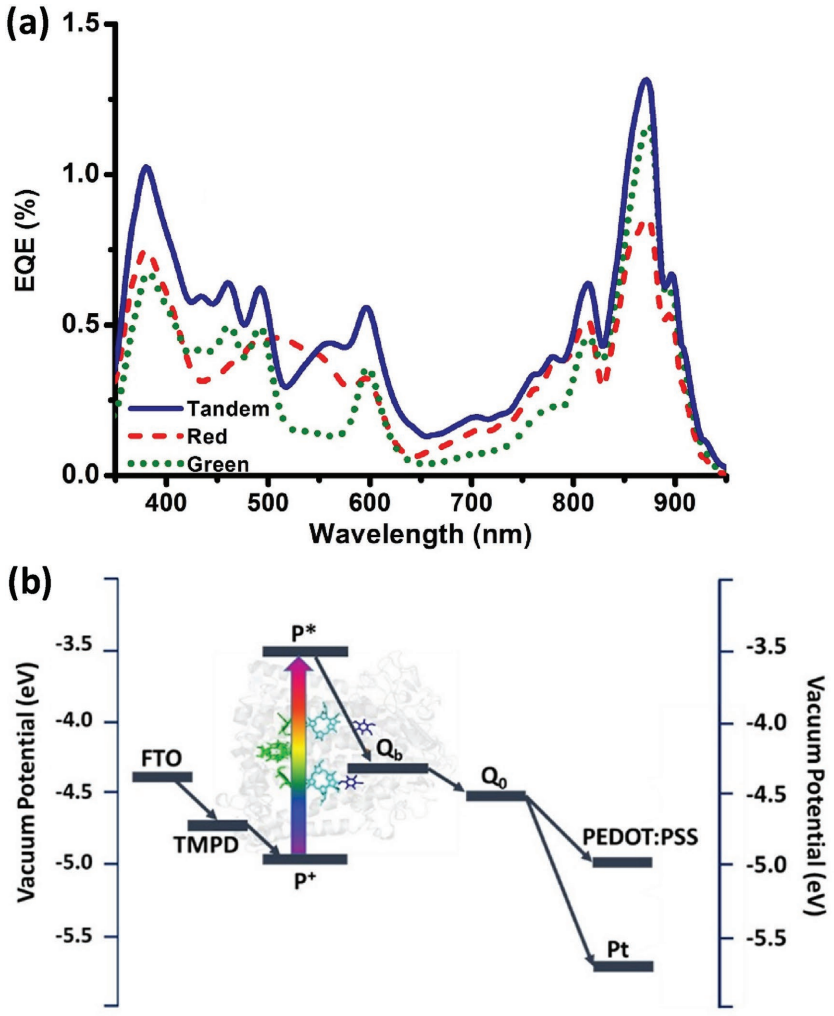

Figure 5. a) EQE action spectra for the red and green sub-cells and the green/red tandem cell. b) Energy level diagram and proposed mechanism of photocurrent generation.

electron transfer from Q_0 (or TMPD) than Pt (Figure 5b), which accounts for the much higher steady-state currents obtained in subcells with PEDOT:PSS as opposed to Pt. The spin coated films of PEDOT:PSS were found to have a smooth and homogeneous surface (Figure 2) which should favor the conductive properties of the film and hence charge transfer.

In the case of this work it was decided to connect the two subcells of the tandem cell in parallel rather than in series. Although both tandem architectures are theoretically proficient in achieving a high light-absorption cross section for a given footprint, output is limited by stringent current-matching criteria. To avoid current losses in parallel-connected tandem cells the component subcells should ideally produce equal photovoltages, whilst to avoid voltage losses in series-connected tandem cells the component subcells should ideally produce equal photocurrents. As the V_{oc} of these biohybrid photoelectrochemical cells is dependent on the energy-levels of the mediators or components of the RC, which are unaltered by a change from red to green light harvesting carotenoids, achieving an approximately equal V_{oc} in the two subcells was easier than achieving an equal J_{sc}, as the latter is affected by the efficiencies of light capture and energy transfer. Hence, the parallel-connected tandem architecture provided the best approach to enhancing the photocurrent generation without altering the footprint of the cell. The modular nature of the LH/RC system in which solar energy harvesting and charge separation are undertaken by different cofactors, enables this approach where these two processes can be manipulated independently of one another. The photocurrent of a parallel-connected tandem cell can be equal to the sum of the two subcell currents if light harvesting by the two is fully complementary. However in the present case the photocurrent of the tandem cell was 12% lower than this sum, which can be attributed to the reduced incident light intensity for the bottom (red) subcell between 400 and 500 nm and also to a minor difference in V_{oc} between the two subcells that results in a circulating current, reducing the overall photocurrent output.

To further examine the relative benefits of a parallel versus serial configuration, a serial green/red tandem cell was fabricated (Figure S4d, Supporting Information) and the J_{SC} and V_{OC} compared to those from green and red subcells. As expected an additive effect on V_{OC} was observed (Figure S8, Supporting Information), but the J_{SC} obtained was lower than for either subcell (Figure S9, Supporting Information), in contrast with the enhancement seen for the tandem cell with the parallel architecture (Figure 4a). The average power density (calculated as the product of J_{SC} and V_{OC}) was 39 nW cm^{-2} in case of the parallel cell and 25 nW cm^{-2} in case of the serial cell.

In conclusion, this work introduced a new approach to photocurrent generation in a biohybrid device by integrating complementary photosynthetic proteins in different layers of a stacked tandem architecture, with the proteins tuned to absorb more photons of a higher energy positioned in the top layer of the device. To realize this, PEDOT:PSS was employed as a cost-effective transparent rear electrode for the cells, which produced the additional benefit of a 12–16-fold enhancement in photocurrent over the Pt electrodes we have used previously. The proof-of-principle tandem biohybrid photoelectrochemical cell constructed using optically-complementary photovoltaic proteins produced a photocurrent that was 88% of the theoretical output of the two component subcells, an output that was higher than could be achieved by simply doubling the amount of either individual protein in the same cell footprint. The complementary absorption characteristics being exhibited only in a narrow wavelength range of 100 nm, a considerable photocurrent addition has been obtained, which indicates the possibility of further enhancement in photocurrent by designing and employing pigment–proteins of wider complementary absorption range. In future

work we will look to achieve higher output by increasing the number of layers and the variety of complementary light-harvesters in the device.

Experimental Section

Biological Material: DNA encoding *pufLM* modified with a polyhistidine tag at the C-terminus of *pufM*[22] was cloned into plasmid pvBALM, which is a derivative of broad-host-range vector pRK415 containing a 6.0 kb section of *Rba. sphaeroides* DNA encoding *pufQBALM*. The resulting plasmid, termed pvBALMt, was introduced into *Rba. sphaeroides* strains DD13 and DD13/G1[18] by conjugative transfer. This produced transconjugant strains expressing His-tagged PufX-deficient RC–LH1 complexes with either red or green carotenoid pigments. Protein complexes were purified as described in detail previously[16] and were stored as concentrated solutions in 20×10^{-3} M Tris (pH 8.0)/0.04% (w/v) DDM at –80 °C. The schematic models of PufX-deficient RC–LH1 complexes in Figure 1 were based on the X-ray crystal structure of the similar complex from *Thermochromatium tepidum*.[10] In some schematics all components other than the carotenoid ring was shown in white. In others the color code was as follows: LH1 α-polypeptide—cyan ribbon; LH1 β-polypeptide—magenta ribbon; LH1 BChls—yellow sticks; RC H-polypeptide—pink surface; RC L-polypeptide—beige surface; RC M-polypeptide—green surface.

Device Fabrication and Characterization: The electrodes were prepared by spin coating two layers of PEDOT:PSS (Clevios PH1000) atop of pre-cleaned substrates. The post-treatment of PEDOT:PSS was done with 8 M methanesulfonic acid at 160 °C following by rinsing with deionized water for three times as reported elsewhere.[23] FTO glasses (2 cm × 2 cm) were cleaned by sequentially sonicating in acetone, isopropyl alcohol, and deionized water before the cell fabrication. The intermediate electrode in the tandem cell was prepared by depositing the same PEDOT:PSS on the nonconductive face of FTO glass. Two rectangular cavities were formed on assembling the three electrodes using a thermoplastic spacer (Surlyn 50 µm) between each pair, followed by heating at 70 °C. After cooling, 5 µL aliquots of protein solution were injected into the top and bottom cavities which were then sealed with epoxy resin. The same procedure was followed for subcells formed from two electrodes. The protein solutions comprised RC–LH1 complexes at a final concentration 50×10^{-6} M, in 20×10^{-3} M Tris (pH 8.0)/0.04% DDM buffer supplemented with 10×10^{-3} M Q_0 and 1×10^{-3} M TMPD. Photocurrents from an active area of 2 mm × 2 mm were measured under white light illumination (100 mW cm^{-2}) using K2400 source meter (Keithley). The absorbance of the protein solutions and the transparency of the cells were measured using a Shimadzu UV-Vis spectrophotometer.

Supporting Information

Supporting Information is available from the Wiley Online Library or from the author.

Acknowledgements

D.J.K.S. and M.R.J. acknowledge the support from the Biotechnology and Biological Sciences Research Council of the UK (project BB/I022570/1). S.K.R. and S.C.T. acknowledge the financial support from MOE AcRF 1 (R-284-000-134-112 and R-284-000-129-133).

Received: August 19, 2016
Revised: October 28, 2016
Published online: December 14, 2016

[1] O. Inganäs, V. Sundström, *Ambio* **2016**, *45*, 15.
[2] C. B. Field, M. J. Behrenfeld, J. T. Randerson, P. Falkowski, *Science* **1998**, *281*, 237.
[3] A. Larkum, *Curr. Opin. Biotechnol.* **2010**, *21*, 271.
[4] a) R. E. Blankenship, D. M. Tiede, J. Barber, G. W. Brudvig, G. Fleming, M. Ghirardi, M. R. Gunner, W. Junge, D. M. Kramer, A. Melis, T. A. Moore, C. C. Moser, D. G. Nocera, A. J. Nozik, D. R. Ort, W. W. Parson, R. C. Prince, R. T. Sayre, *Science* **2011**, *332*, 805; b) G. D. Scholes, G. R. Fleming, A. Olaya-Castro, R. van Grondelle, *Nat. Chem.* **2011**, *3*, 763; c) N. S. Lewis, D. G. Nocera, *Proc. Natl. Acad. Sci. USA* **2006**, *103*, 15729; d) W. Wang, H. Wang, Q. Zhu, W. Qin, G. Han, J. R. Shen, X. Zong, C. Li, *Angew. Chem. Int. Ed.* **2016**, *55*, 9229; e) W. Wang, J. Chen, C. Li, W. Tian, *Nat. Commun.* **2014**, *5*, 4647; f) S. Y. Lee, S. Y. Lim, D. Seo, J. Y. Lee, T. D. Chung, *Adv. Energy Mater.* **2016**, *6*, 1502207.
[5] R. Croce, H. van Amerongen, *Nat. Chem. Biol.* **2014**, *10*, 492.
[6] a) P. Heathcote, M. R. Jones, The Structure-Function Relationships of Photosynthetic Reaction Centers, *Comprehensive Biophysics*, Elsevier, Amsterdam **2012**, p. 115; b) R. E. Blankenship, *Molecular Mechanisms of Photosynthesis*, second, John Wiley & Sons, UK **2014**.
[7] S. K. Ravi, S. C. Tan, *Energy Environ. Sci.* **2015**, *8*, 2551.
[8] a) D. Gerster, J. Reichert, H. Bi, J. V. Barth, S. M. Kaniber, A. W. Holleitner, I. Visoly-Fisher, S. Sergani, I. Carmeli, *Nat. Nanotechnol.* **2012**, *7*, 673; b) O. Yehezkeli, R. Tel-Vered, J. Wasserman, A. Trifonov, D. Michaeli, R. Nechushtai, I. Willner, *Nat. Commun.* **2012**, *3*, 742; c) K. Hasan, E. Çevik, E. Sperling, M. A. Packer, D. Leech, L. Gorton, *Adv. Energy Mater.* **2015**, *5*, 1501100.
[9] G. Feher, J. P. Allen, M. Okamura, D. Rees, *Nature* **1989**, *339*, 111.
[10] S. Niwa, L.-J. Yu, K. Takeda, Y. Hirano, T. Kawakami, Z.-Y. Wang-Otomo, K. Miki, *Nature* **2014**, *508*, 228.
[11] Y. Kim, S. A. Shin, J. Lee, K. D. Yang, K. T. Nam, *Nanotechnology* **2014**, *25*, 342001.
[12] O. Yehezkeli, R. Tel-Vered, D. Michaeli, I. Willner, R. Nechushtai, *Photosynth. Res.* **2014**, *120*, 71.
[13] a) M.-J. den Hollander, J. G. Magis, P. Fuchsenberger, T. J. Aartsma, M. R. Jones, R. N. Frese, *Langmuir* **2011**, *27*, 10282; b) R. Caterino, R. Csiki, A. Lyuleeva, J. Pfisterer, M. Wiesinger, S. D. Janssens, K. Haenen, A. Cattani-Scholz, M. Stutzmann, J. A. Garrido, *ACS Appl. Mater. Interfaces* **2015**, *7*, 8099; c) J. Gebert, C. Reiner-Rozman, C. Steininger, V. Nedelkovski, C. Nowak, C. A. Wraight, R. L. Naumann, *J. Phys. Chem. C* **2015**, *119*, 890; d) M. Kondo, K. Iida, T. Dewa, H. Tanaka, T. Ogawa, S. Nagashima, K. V. P. Nagashima, K. Shimada, H. Hashimoto, A. T. Gardiner, R. J. Cogdell, M. Nango, *Biomacromolecules* **2012**, *13*, 432; e) H. Yaghoubi, Z. Li, D. Jun, R. Saer, J. E. Slota, M. Beerbom, R. Schlaf, J. D. Madden, J. T. Beatty, A. Takshi, *J. Phys. Chem. C* **2012**, *116*, 24868; f) A. Takshi, J. D. Madden, J. T. Beatty, *Electrochim. Acta* **2009**, *54*, 3806.
[14] S. C. Tan, L. I. Crouch, M. R. Jones, M. Welland, *Angew. Chem. Int. Ed.* **2012**, *51*, 6667.
[15] a) S. C. Tan, L. I. Crouch, S. Mahajan, M. R. Jones, M. E. Welland, *ACS Nano* **2012**, *6*, 9103; b) S. C. Tan, F. Yan, L. I. Crouch, J. Robertson, M. R. Jones, M. E. Welland, *Adv. Funct. Mater.* **2013**, *23*, 5556.
[16] V. M. Friebe, J. D. Delgado, D. J. Swainsbury, J. M. Gruber, A. Chanaewa, R. van Grondelle, E. von Hauff, D. Millo, M. R. Jones, R. N. Frese, *Adv. Funct. Mater.* **2016**, *26*, 285.
[17] a) P. K. Dutta, S. Lin, A. Loskutov, S. Levenberg, D. Jun, R. Saer, J. T. Beatty, Y. Liu, H. Yan, N. W. Woodbury, *J. Am. Chem. Soc.* **2014**, *136*, 4599; b) I. Nabiev, A. Rakovich, A. Sukhanova, E. Lukashev, V. Zagidullin, V. Pachenko, Y. P. Rakovich, J. F. Donegan,

A. B. Rubin, A. O. Govorov, *Angew. Chem. Int. Ed.* **2010**, *49*, 7217; c) F. Milano, R. R. Tangorra, O. Hassan Omar, R. Ragni, A. Operamolla, A. Agostiano, G. M. Farinola, M. Trotta, *Angew. Chem. Int. Ed.* **2012**, *51*, 11019; d) E. Maksimov, E. Lukashev, N. K. Seifullina, G. Nizova, V. Pashchenko, *Nanotechnol. Russ.* **2013**, *8*, 423; e) P. K. Dutta, S. Levenberg, A. Loskutov, D. Jun, R. Saer, J. T. Beatty, S. Lin, Y. Liu, N. W. Woodbury, H. Yan, *J. Am. Chem. Soc.* **2014**, *136*, 16618.

[18] M. R. Jones, G. Fowler, L. Gibson, G. G. Grief, J. Olsen, W. Crielaard, C. Hunter, *Mol. Microbiol.* **1992**, *6*, 1173.

[19] S. C. Chi, D. J. Mothersole, P. Dilbeck, D. M. Niedzwiedzki, H. Zhang, P. Qian, C. Vasilev, K. J. Grayson, P. J. Jackson, E. C. Martin, *Biochim. Biophys. Acta, Bioenerg.* **2015**, *1847*, 189.

[20] a) D. Alemu, H.-Y. Wei, K.-C. Ho, C.-W. Chu, *Energy Environ. Sci.* **2012**, *5*, 9662; b) D. H. Yoon, S. H. Yoon, K.-S. Ryu, Y. J. Park, *Sci. Rep.* **2016**, *6*, 19962.

[21] Y. Xia, J. Ouyang, *J. Mater. Chem.* **2011**, *21*, 4927.

[22] D. J. Swainsbury, V. M. Friebe, R. N. Frese, M. R. Jones, *Biosens. Bioelectron.* **2014**, *58*, 172.

[23] J. Ouyang, *ACS Appl. Mater. Interfaces* **2013**, *5*, 13082.

